Fluid Mechanics Research Journal
Vol. 1, No. 1; 2019
Published by CanSRG
http://www.cansrg.com/journals/fmrj/

Comparison of the Turbulent Length Scales of Three Different Boundary Layers within a Compressible Flow Facility

Peter J Disimile[1] and Norman Toy[2,*]

[1]*Department of Aerospace Engineering, University of Cincinnati, Cincinnati, Ohio 47006, USA*
[2]*Engineering & Scientific Innovations Inc, 7383 Dixie Hwy, Fairfield, OH 45014, USA*

Abstract

Three different turbulent boundary layers have been generated within a low speed compressible flow facility and the Kolmogorov, Taylor and the Integral length scales were determined. One of the boundary layers was allowed to develop naturally, with a second one being produced by a trip and vortex generators, and with the third one by including a uniform surface roughness downstream of the vortex generators. A temperature compensated single hot-wire probe, operating at a sampling frequency of 45 kHz, was used to acquire turbulent boundary layer data from a single location. It was found that evidence of the turbulent generating devices was readily discernible in the turbulent boundary layer and could be identified within the Taylor and the Integral length scales but not for the Kolmogorov scales although their effect was detected.

Keywords: *Turbulent boundary layers; length scales; dissipation rates.*

Nomenclature

C_f	Friction Coefficient
H	Shape Factor
M	Mach number
Re	Reynolds Number
U	Freestream Velocity
u	Instantaneous Velocity
u’	rms Velocity
u^*	Friction Velocity
u^+	Non-dimensional Velocity in terms of friction velocity
y	Height above the floor of the channel
y^+	Non-dimensional wall coordinates

Greek symbols

δ	Boundary Layer thickness
δ^*	Displacement Thickness
ε	Dissipation
ε(ν)	Viscous Dissipation
ε(I)	Inertia Dissipation
η	Kolmogorov Length Scale
θ	Momentum Thickness
κ	Von Karman Constant
Λ	Integral Length Scale
λ	Taylor Length Scale
μ	Dynamic Viscosity
ν	Kinematic Viscosity (corrected for pressure and temperature using Sutherland’s equation)
ρ	Density of air
τ	Shear Stress

1. Introduction

There are many instances where a turbulent boundary layer occurs and give rise to fluid mechanic problems. However, not all turbulent boundary layers may be seen as being ‘well-developed’ but are more-often-than-not highly turbulent flows with origins determined from upstream obstacles. For example, the flow over a large flat roof that has protuberances on its surface, such as ventilation or window/configurations, may have a boundary layer growing over its surface but which will not be fully developed and which may impede (or assist) the overall effect of the ventilation equipment; or in ducted flows in which a ‘fire’ has developed accidently, due to possible hot surface ignition, and where the boundary layer may be considered turbulent

* Corresponding author
Submitted: September 30, 2019 Accepted: December 4, 2019

although not classified as fully developed. In such instances, turbulent length scales are important in defining the state of the turbulent boundary layer and how the flow dynamics may impact the ensuing fluid mechanics.

This is especially true for studies relating to the air-wake downstream of the superstructure of a naval vessel and its effect on the landing and take-off from the landing zone by helicopter pilots. In most experimental studies of this particular problem the flow field has been considered as that developing from a backward facing step and its associated recirculation zone without due consideration to the complex flow field upstream of the step, Shafer [1], Bardera Mora [2].

Although there have been a number of studies involving wall bounded shear flows, Wosniak [3], Buschmann and Gad-el-Hak [4] and turbulent boundary layers over hydraulically smooth and rough surfaces, Schultz and Flack [5], few studies have detailed the scaling properties of a turbulent boundary layer that has turbulent intensity values that increase within the boundary layer thickness.

Imprecise data is often recorded or provided in an experimental investigation because of the necessary time needed to undertake comprehensive turbulence scale data, including the experimental design period and the method of data acquisition and analysis. This may result in general approximations being utilized in a computational model without rigorous validation of the turbulence properties. For complex flows where a turbulent boundary layer is compromised by upstream obstacles, it is even more important to undertake exhaustive flow analysis including the length scales of the turbulent structures within the flow regime. This paper seeks to address some of these issues by providing a clear set of turbulent length scales, namely, the Kolmogorov, Taylor and Integral length scales for three different boundary layer developments within a high speed, mildly compressible, subsonic channel flow.

2. Experimental Facility

A high-speed, open loop, suction wind tunnel was fabricated using a 2.8 m^3/s centrifugal blower to draw laboratory air through an inlet duct into an acrylic test section with an attached diffuser, exhausting the air back into the laboratory, Figure 1. An inlet bell mouth provided a smooth transition from the laboratory into the inlet duct section, thereby minimizing freestream turbulence, while an exhaust duct was used to direct exhaust air away from the inlet to reduce interference effects.

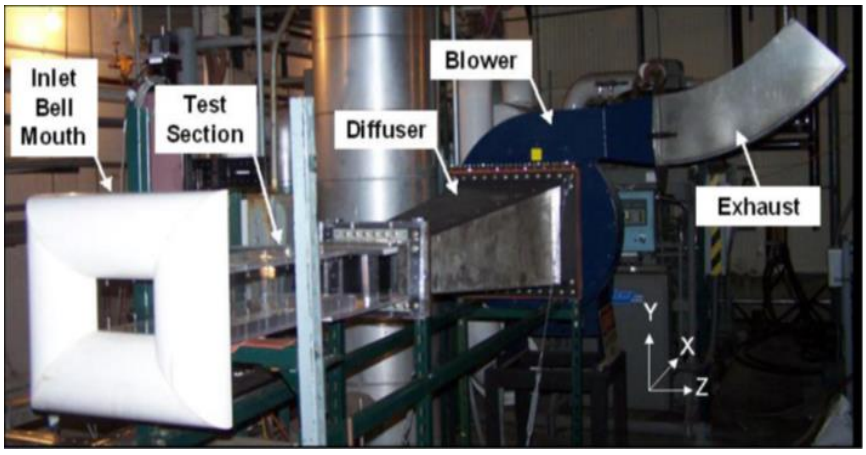

Figure 1. Experimental Facility.

The test section was initially designed as a two-dimensional backward facing step arrangement, and was fabricated from transparent acrylic to allow unobstructed optical access, Figure 2. However, the inlet duct section upstream of the step provided an opportunity to explore the effect of generating different turbulent boundary layers, and therefore different turbulent length scales. The inlet duct section has a height of 104.4 mm, a width of 175.0 mm and a length of 762.0 mm. This cross section was specifically chosen to achieve airspeeds of approximately Mach 0.5, given the blower specifications, while the length was selected to allow sufficient streamwise distance for boundary layer development. At the location of the step, the height of the test section suddenly expands to 139.7 mm, while the test section width remains constant, Disimile et al [6]. This produces a two-dimensional step flow with a step height of 35.3mm, but is not used in this experimental analysis. In order to achieve different turbulent boundary layers within this configuration, three different fetch configurations were developed.

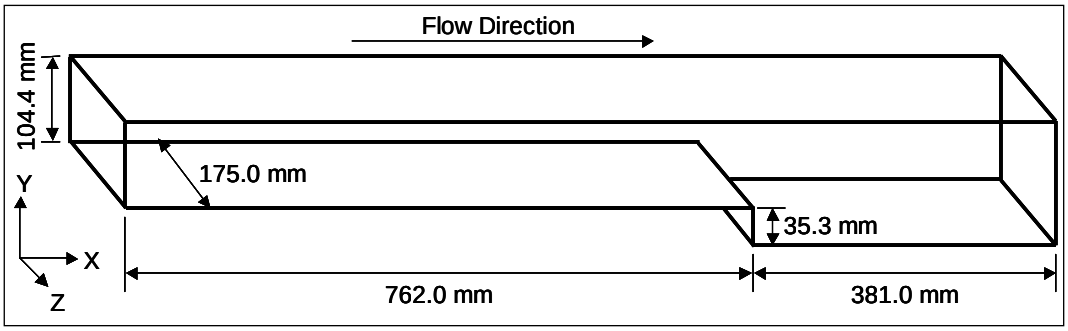

Figure 2. Test Section Schematic.

The first boundary layer (BL1) was simply developed through a clean tunnel such that the freestream air was drawn in through the bell mouth and allowed to develop naturally up to the backward facing step edge. The second boundary layer (BL2) was developed by designing and constructing a small, sharp edged, 8 mm high fence at the start of the channel section in order to trip the incoming flow, followed by a set of 8 vortex-developing spires of dimensions shown in Figure 3 that spanned the width of the channel section.

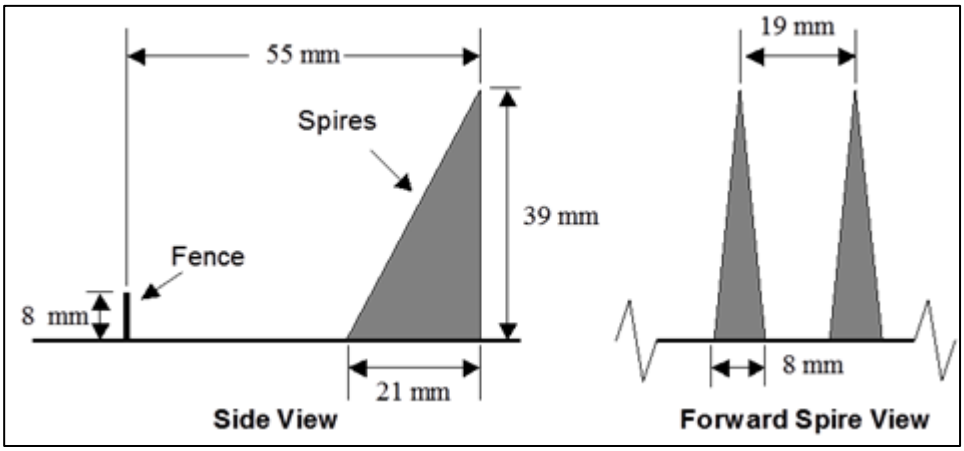

Figure 3. Two-Stage Boundary Layer Modification Diagram.

The third boundary layer (BL3) was developed by increasing the surface roughness of the fetch

downstream of the spires and was constructed of small squares obstacles evenly distributed throughout the channel floor with dimensions as shown in Figure 4. Figure 5 provides an overview of the entire boundary layer producing modifications.

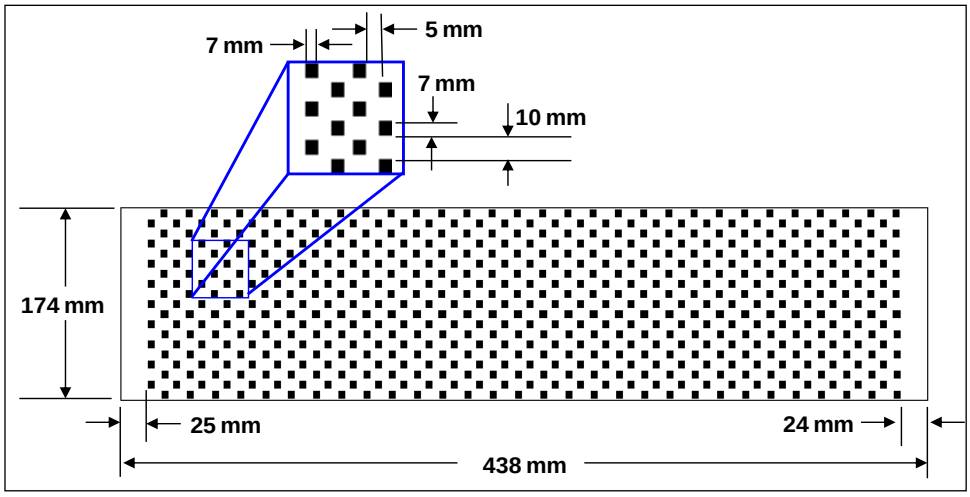

Figure 4. Diagram of Surface Roughness Grid.

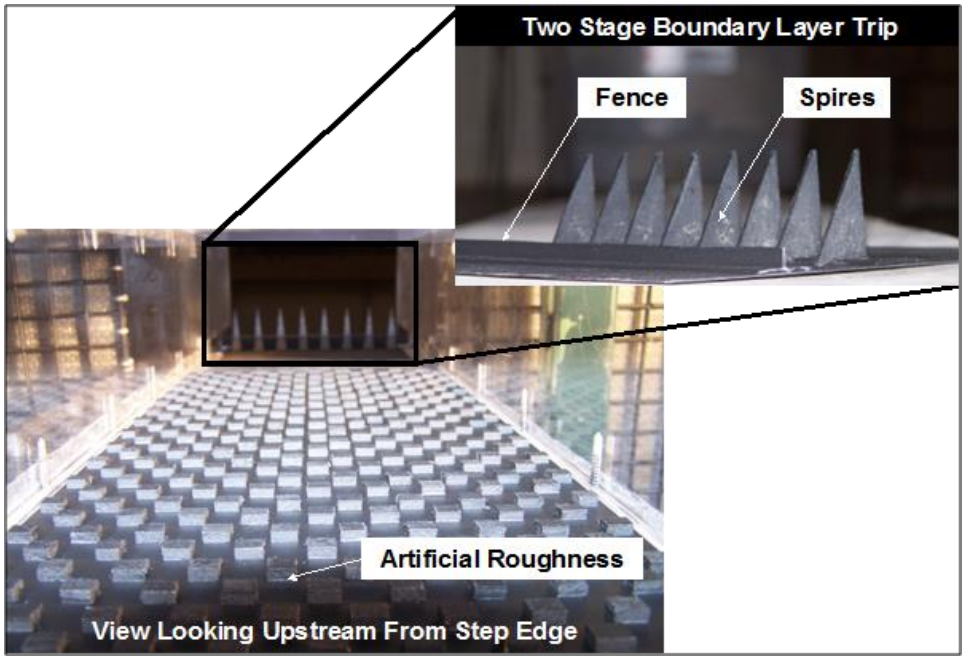

Figure 5. Boundary Layer Modifications (Boundary Layer 3).

Although the freestream channel flow for the clear tunnel could be as high as 185 m/s (M ~ 0.53), it was decided to operate at a lower freestream velocity of 168 m/s (M~ 0.49) because of the constraints the thickness of the expected two larger boundary layers (BL2 & BL3) would have on the flow geometry at the measuring site. The site chosen for all measurements of the boundary layers was at a position on the test section centre line, 17.7 mm upstream of the edge of the backward facing step (half a step height). The channel flow also provided a slightly favorable pressure gradient (dp/dx) of approximately 17.8 kPa/m.

All velocity and turbulence measurements were acquired with a constant temperature anemometry system (CTA) utilizing a 5 μm diameter Tungsten hot-wire sensor with a length/diameter ratio of 250, and a miniature high speed Type K bare-bead thermocouple attached to the probe support. This thermocouple allowed the local temperature of the flow to be monitored thereby allowing simultaneous temperature corrections to be made to the hot wire data. The hot-wire data was acquired at a sampling rate of 45 kHz for 20 seconds ensuring a sufficient time response and acceptable stationary averages of all quantities. It should be noted that the thermal correction applied to the CTA data, which is due to the temperature difference between the air temperature at calibration of the hot-wire and the temperature within the boundary layer, was applied as documented in DANTEC, [7], and provided a velocity data set with a maximum error of +/- 1%.

A three-axis, computer controlled, traversing system was used in order to acquire repeatable positioning of the hot-wire and thermocouple probe within the boundary layers and was capable of providing a resolution of 22 μm. Measurements were commenced with the probe located 30 μm above the floor of the test section, which was confirmed with an optical measuring system, and variable locations , ranging from 0.1 mm in the high shear regions to 5.0 mm close to the boundary layer height, provided a full set of velocity and turbulent intensity data, taking into account resolution issues as outlined in Hutchins et al [8].

3. Discussion

Integration of the velocity profiles and applying the u/U ~ 0.99 rule allowed the boundary layer thickness (δ) of the three boundary layers to be calculated, along with the displacement thickness (δ^*) and the momentum thickness (θ) for the freestream values as shown in Table 1. Included in this table is the shape parameter (H) and although it increases with the type of boundary layer development the values are still within acceptable limits.

Table 1. Details of the Three Boundary Layers.

	Configuration		
	BL1	BL2	BL3
δ (mm)	31.6	50.3	57.3
δ* (mm)	2.4	8.6	11.7
θ (mm)	1.9	6.5	7.7
H	1.26	1.32	1.52
U (m/s)	168	167	165.5

Figure 6 provide detailed normalized velocity profiles of the three different boundary layers and shows how the initial clean channel velocity profile (BL1) is close to that of a power-law velocity profile ($u/U = (y/\delta)^{1/n}$) where the exponent 'n' is close to the value of 10 rather than the normally fully developed turbulent boundary layer of 7. However, this is explainable since it is recognized that the exponent 'n' is Reynolds Number (Re) dependent and for high values of Re, greater than10^6, a higher value of 'n' is justifiable as it is in this case.

The boundary layers produced by the addition of the trip and vortex generators (BL2) and the uniformly distributed roughness (BL3) redistributes the energy within the boundary layer and it no longer follows a normal fully developed turbulent boundary layer. However, the early start of

this second boundary layer profile (BL2) begins similar to that of (BL1) but rapidly changes at approximately $y/\delta = 0.11$ where the wake effect of the trip and the vortex generators begin to be felt within the boundary layer and continues with a reduced velocity until it reaches the edge of the boundary layer at $y/\delta = 1.0$.

The third boundary layer (BL3) shows how the uniform roughness has affected the initial start of the boundary layer, starting at a reduced velocity of approximately $u/U = 0.4$, and increases in value, roughly linearly, up to a value of $y/\delta = 0.4$ where it is then affected by the outer-part of the wake from the vortex generators and from there on follows a profile similar to that of (BL2). The turbulence profiles of these three distinct boundary layers provides even more information as to how the trip, vortex generators and the uniform roughness has affected the initial, clean channel, boundary layer.

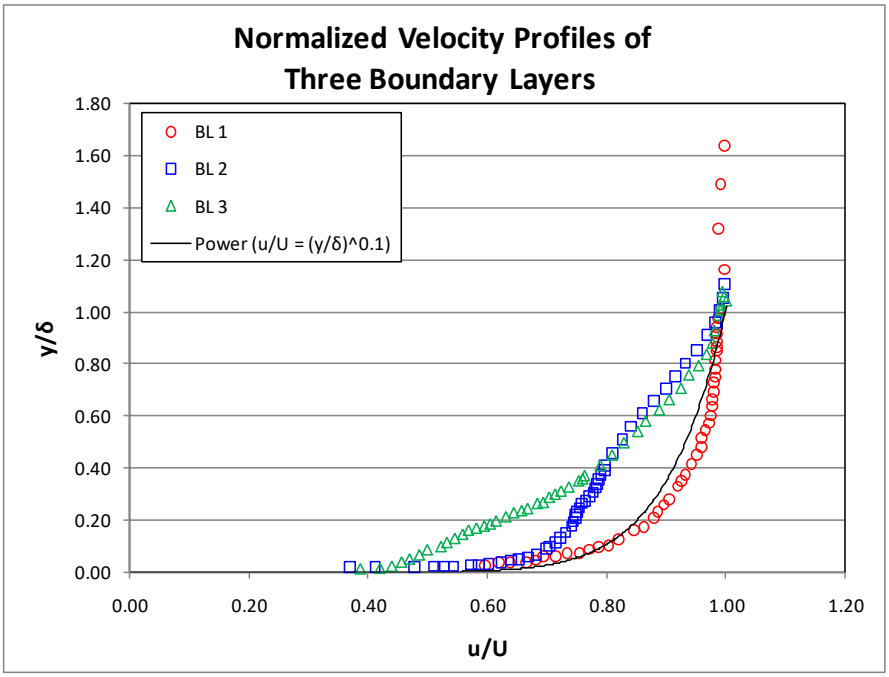

Figure 6. Boundary Layer Profiles of the Three Boundary Layers.

The turbulence intensity of the boundary layer of the clean channel (BL1) is shown in Figure 7. Here it can be observed that, in most part, it is behaving as a fully developed boundary layer with a maximum value of about 0.07 close to the channel wall, reducing in value to approximately 0.01 at the edge of the boundary layer at $y/\delta = 1.0$. The turbulence intensity of BL2 and BL3 boundary layers are substantially different with BL2 following the trend of BL1 up to a value of approximately $y/\delta = 0.2$ and then it deviates, increasing in value up to $y/\delta = 0.78$ where it then reduces as the edge of the boundary layer approaches. The location of these changes in turbulence intensity may be attributed to the wake effects, first, of the 8 mm high trip at the mouth of the channel section (trip height / δ of BL2 ~ 0.16), and secondly, the 39 mm height of the vortex generators (generator height / δ of BL2 ~ 0.78).

The turbulence intensity of BL3 may be observed to start at a value similar to that for BL1 and BL2 at approximately 0.07 but then increases. This increase in turbulence intensity close to the wall may be attributed to the distributed roughness and it only starts to reduce when the effect of

the wake of the trip is experienced at approximately y/δ = 0.15 (given by trip height / δ for BL3 ~ 0.14). This distributed roughness appears to have added turbulence to the lower part of the boundary layer up to approximately y/δ = 0.50 and this has affected the entire boundary layer development. Above this maximum turbulence intensity at y/δ = 0.15 the turbulence intensity falls monotonically up to the edge of the boundary layer at a relatively constant rate between y/δ = 0.20 and y/δ = 0.60 and again between y/δ = 0.80 and y/δ = 1.00. However, between the values of y/δ = 0.60 and y/δ = 0.80, the turbulence intensity falls at more than twice this rate and is considered to be due to the effect of the tip vortices being shed by the vortex generators, and adding to the increase in turbulence at this level.

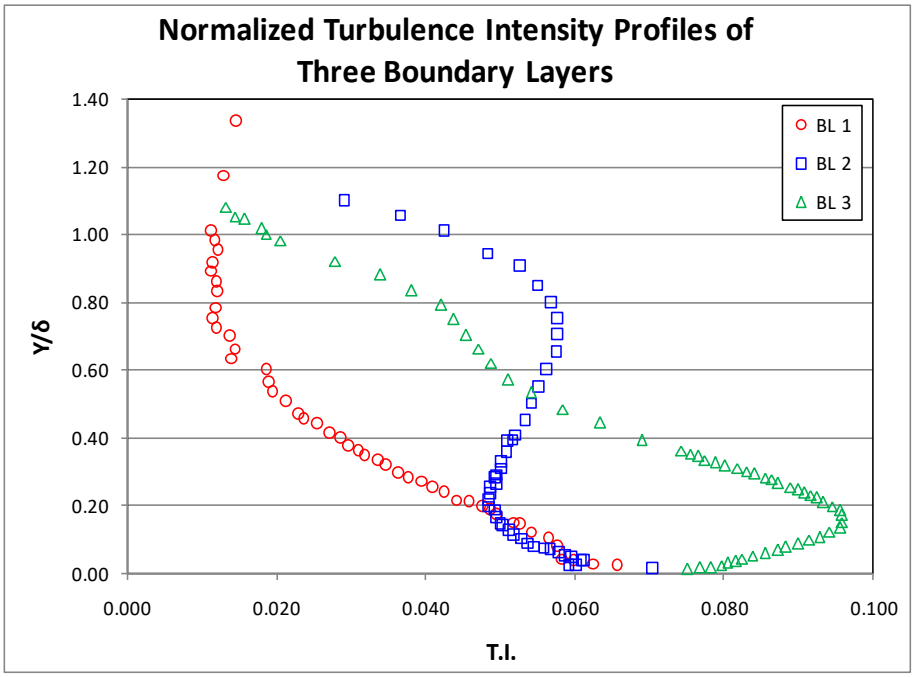

Figure 7. Turbulent Intensity Profiles of the Three Boundary Layers.

In order to provide further insight into how these three boundary layers are affected by the inclusion of turbulence generating obstructions a study was undertaken of the turbulence length scales that were produced. However, although there are a number of different methodologies for determining the turbulent length scales from experimental data the method chosen for this study were based on the Kolmogorov length scales and the Reynolds number scaling relationships of Taylor and the Integral length scales by calculating them from direct measurement of the dissipation rate. This methodology had a number of advantages, namely,

- Isotropy of the small scales is highly likely (although that of the large scales may not be assumed in a turbulent boundary layer), and
- Ascertaining the Taylor and Integral length scales from the autocorrelation of the velocity data is vulnerable to external interferences which could lead to skewing of the autocorrelation function.

The turbulence length scales within these three boundary layers were considered to be dependent on the energy dissipation rate (ε) which could be derived from the viscous term ε(ν), (Eqn. 1) as well as from an inertia term ε(I), (Eqn. 2).

$$\varepsilon(\nu) = \frac{u^{*3}}{\kappa y} \tag{1}$$

$$\varepsilon(I) = \frac{\overline{d(u')^2}}{dt} \tag{2}$$

For the small scale turbulence, the Kolmogorov length scales (η), were determined from the following expression, (Eqn. 3).

$$\eta = \left[\frac{\upsilon^3}{\varepsilon}\right]^{1/4} \tag{3}$$

and the larger length scales of Taylor (λ), and the Integral length scale (Λ), determined from the Reynolds number scaling relationships as given by Tennekes and Lumley [9], (Eqn.s 4 and 5).

$$\frac{\lambda}{\eta} \approx 15^{1/4} Re_\lambda^{1/2} \quad where \quad Re_\lambda = \frac{u'\lambda}{\upsilon} \tag{4}$$

And

$$\frac{\lambda}{\Lambda} \approx Re_\Lambda^{-1/2} \quad where \quad Re_\Lambda = \frac{u'\Lambda}{\upsilon} \tag{5}$$

Since the viscous dissipation rate and the length scales are all dependent on the friction velocity (u*), this was determined, along with the local skin friction coefficient (C_f), from the experimental data of the three boundary layers, Clauser [10], and the values presented in Table 2. This was achieved by considering the following log-law of the wall (Eqn. 6) and plotting the non-dimensional velocity data (u/U) against the logarithmic position in the boundary layer, and determining the friction velocity from the slope of the data, Figure 8.

$$\frac{u}{U} = \frac{2.5u^*}{U} ln\left(\frac{yU}{\nu}\right) + A \tag{6}$$

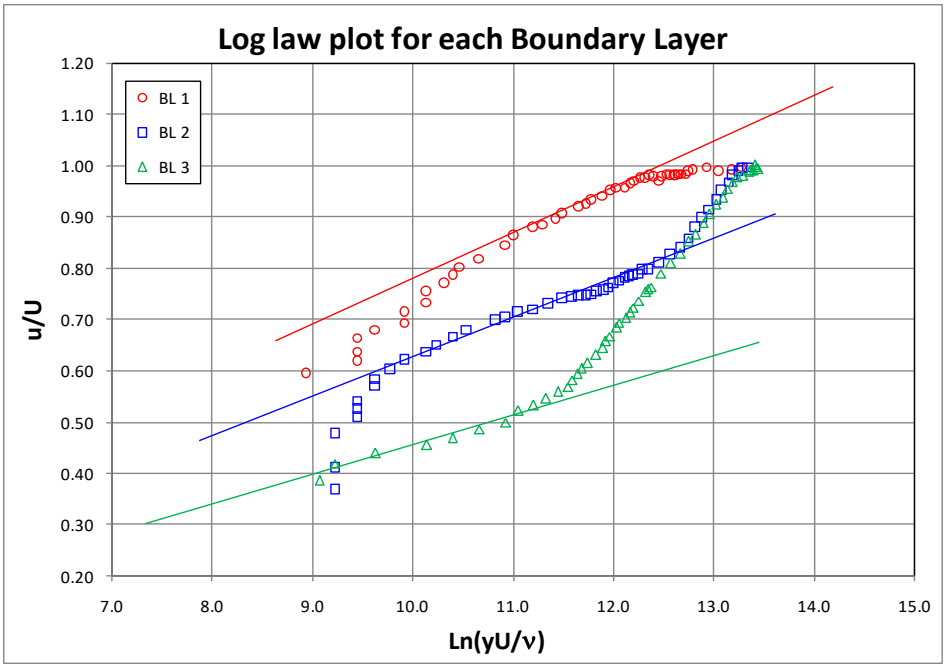

Figure 8. Log-law plot of the velocity data for each of the Three Boundary Layers.

It should be noted that the friction velocity (u*) for the distributed roughness case (BL3) was substantially lower than that for the clean tunnel (BL1) even though the roughness increased the turbulence intensity close to the channel surface, Figure 7. Since the local skin friction

coefficient is related to the local shear stress (τ) and this is dependent on the expression $u^* = \sqrt{(\tau/\rho)}$, it follows that the local skin friction coefficient will reduce as the turbulence increased in the boundary layer and these values are given in Table 2. However, Table 2 also shows that the local friction coefficient falls as the Reynolds number based on momentum thickness (Re_θ) increases in value and it does so at a much higher rate than that given in the literature for a favorable pressure gradient.

Table 2. Friction Velocity and Friction Coefficient of the three boundary layers.

	Configuration		
	BL1	BL2	BL3
u* (m/s)	6.05	5.04	3.70
C_f	0.0026	0.0018	0.0010
Re_θ	21280	72800	86240

Furthermore, the velocity profiles were re-plotted in terms of the non-dimensional wall coordinates

$$u^+ = \left[\frac{U}{u^*}\right] \quad \text{and} \quad y^+ = \left[\frac{y\,u^*}{\nu}\right] \tag{7}$$

to ensure that the boundary layers were comparable to the Law of the Wall, as well as being compared with previously published data of Marusic et al [11] and Monty et al [12], Figure 9. All three boundary layers were in agreement with the Law of the Wall as well as the published data but with some difference in BL2 and BL3. Both of these boundary layers provide clear evidence of the wake effect from the trip and the vortex generators (BL2) and very substantially the added uniform roughness (BL3).

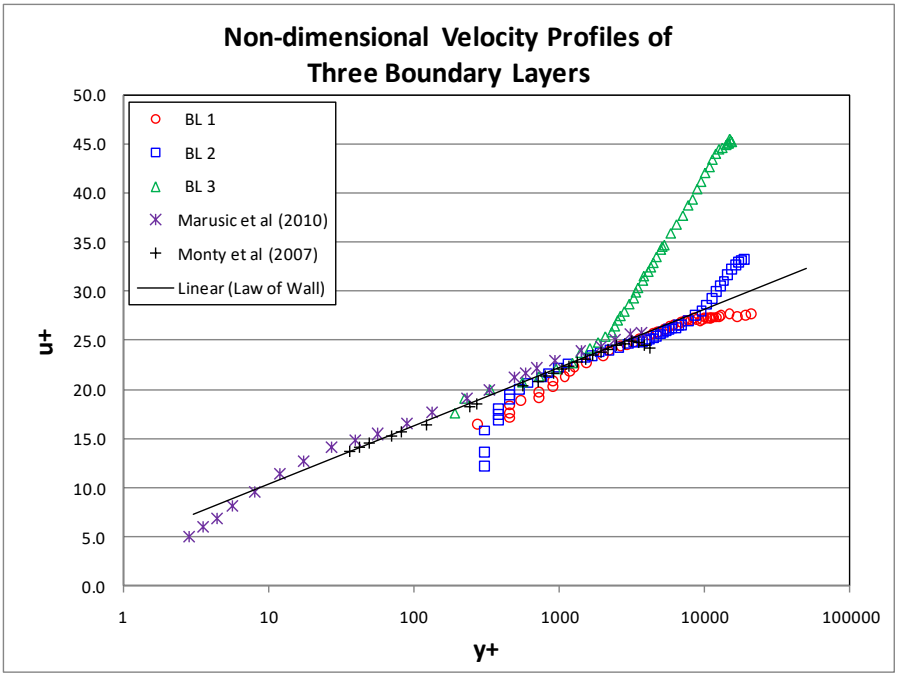

Figure 9. Non-dimensional Velocity Profiles of the Three Boundary Layers.

How the dissipation rate changes through the boundary layer is shown in Figure 10 for the Viscous and Inertia Dissipation, Eqn. (1) & (2), for all three boundary layers. Obviously, the

Viscous Dissipation, ε(ν), falls linearly since this is only dependent on the location within the boundary layer but it may be observed that as the turbulence intensity increases throughout the boundary layer, BL2 and BL3, the rate of energy dissipation is lower. However, the same cannot be said of the Inertia Dissipation, ε(I), where it may be seen that the energy is approximately the same for all three boundary layers close to the wall at y+ = 200, with the BL1 and BL2 falling at the same rate up to y+ = 2500, whereupon the dissipation in BL1 suddenly falls at a relatively high rate up to y+ = 9000 and then plateaus as the edge of the boundary layer is approached at y+ =13000. The energy within BL2 however, remains approximately constant throughout the boundary layer, unlike that of BL3 that increases slightly up to y+ = 3500 and then falls at different rates as the edge of the boundary layer approaches.

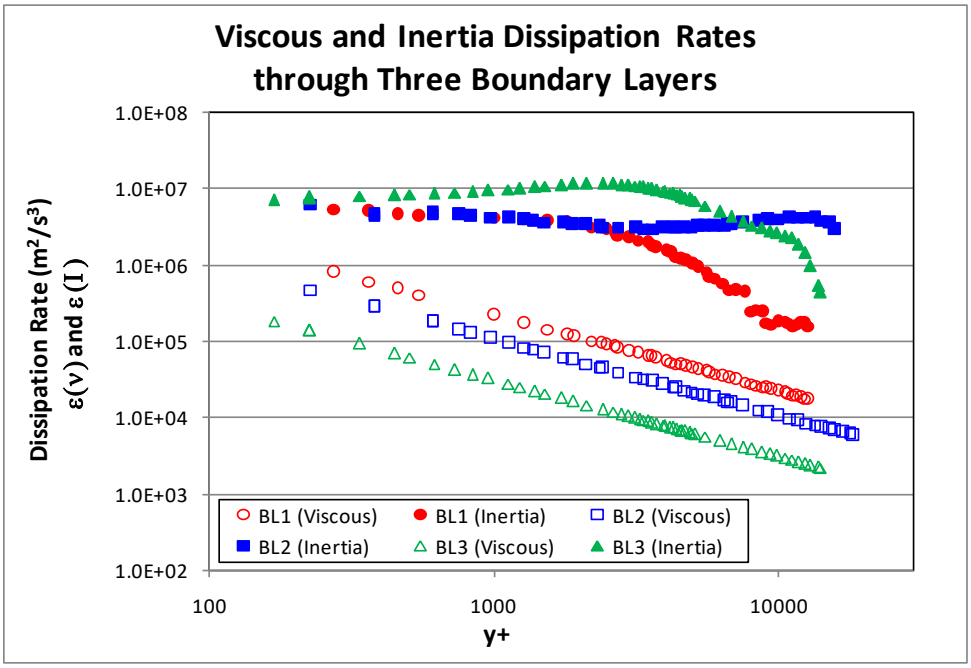

Figure 10. Viscous and Inertia Dissipation Rates through Three Boundary Layers.

Since the Kolmogorov length scales are only concerned with the viscous dissipation through the boundary layers, that is,

$$\eta\left(\varepsilon\left(\nu\right)\right) = \left[\frac{\nu^3}{\varepsilon(\nu)}\right]^{1/4}$$

Figure 11 illustrates how these length scales increase as the turbulence intensity increases for each of the boundary layers as well as the size of the scales due to viscous dissipation. The length scales for the clean tunnel, BL1, only increases from about 8μm to 21μm throughout the boundary layer whereas that for BL2 and BL3, where the turbulence intensity has been boosted by the trip and vortex generators, the length scales increases from 9 μm to 27 μm and from 12 μm to 36 μm, respectively.

On a logarithmic scale, these Kolmogorov lengths are shown to be linear with respect to the non-dimensional wall units, Figure 12.

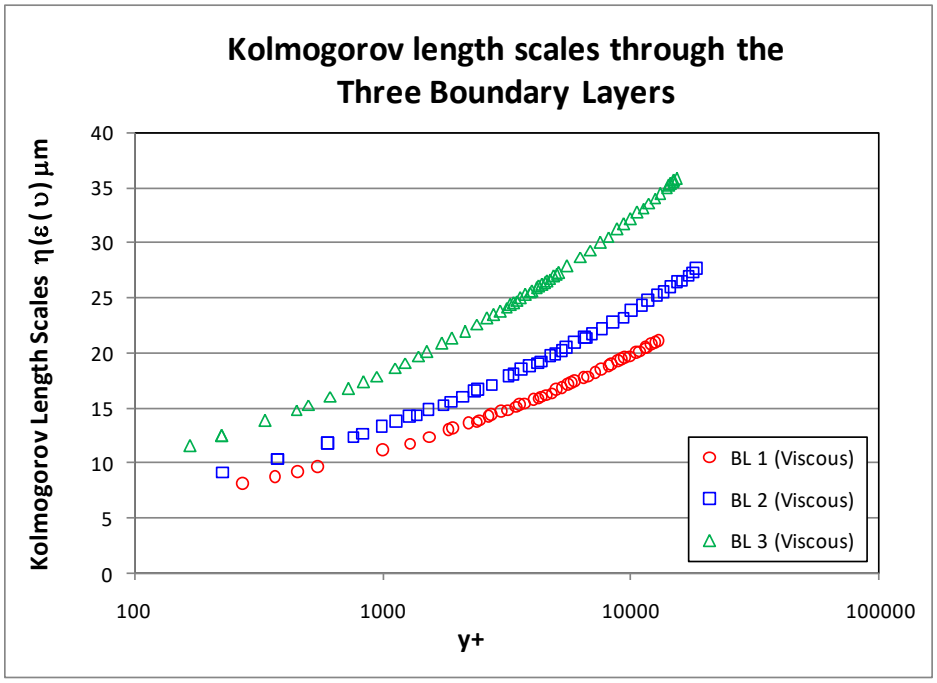

Figure 11. Kolmogorov Length Scales of Three Boundary Layers using Viscous Dissipation Rate.

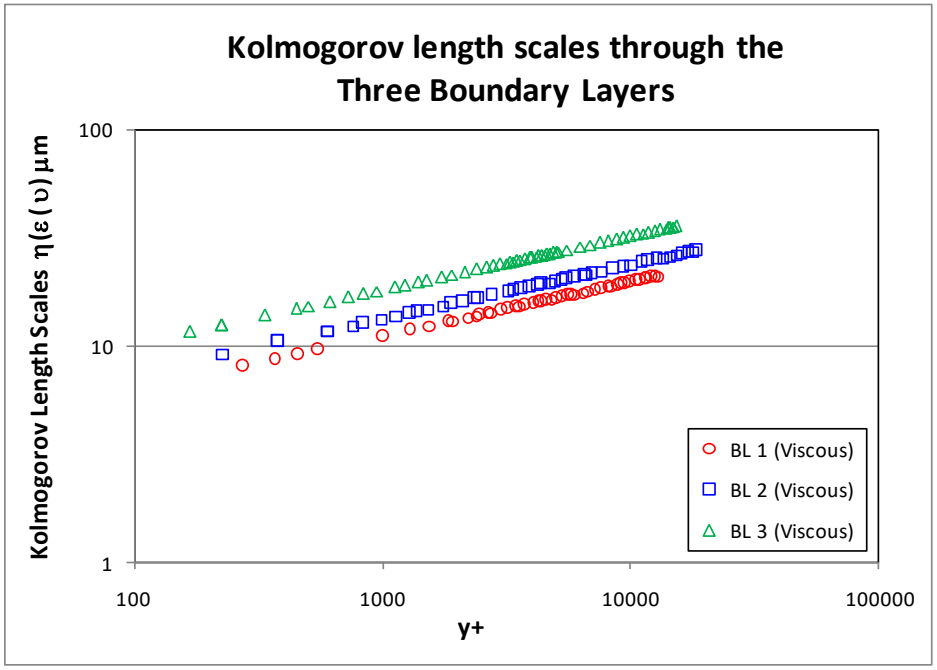

Figure 12. Logarithmic Kolmogorov Length Scales of Three Boundary Layers using Viscous Dissipation Rate.

The Taylor length scales rely on the values of the Kolmogorov scales to be determined and are known to be of intermediate value between the Kolmogorov and the Integral length scales. For this analysis the Taylor scales were determined from Eqn. 4 and are shown in Figure 13 and plotted logarithmically against the non-dimensional wall units. Here, it may be observed that once again the increase in turbulence intensity through the boundary layer notably increases the length scales in a similar, although nonlinear manner, to that of the Kolmogorov scales but with a

substantial increase in value. For example, the clean tunnel boundary layer, BL1, increases from about 180 µm to 400 µm at the early stage of the boundary layer development and then falls as the boundary layer grows, some 20 times larger than the Kolmogorov length scales. The Taylor scales for the more turbulent boundary layers, BL2 and BL3, increases in a similar fashion with BL3 peaking at a length scale of approximately 2500 µm, whereas that for BL2 was 1600 µm. however, both of these highly turbulent boundary layers show a rapid reduction in the length scales as the edge of the boundary layer approaches which is to be expected since the turbulence intensity outside of the boundary layer is considerable less than that within these two particular boundary layers, Figure 7.

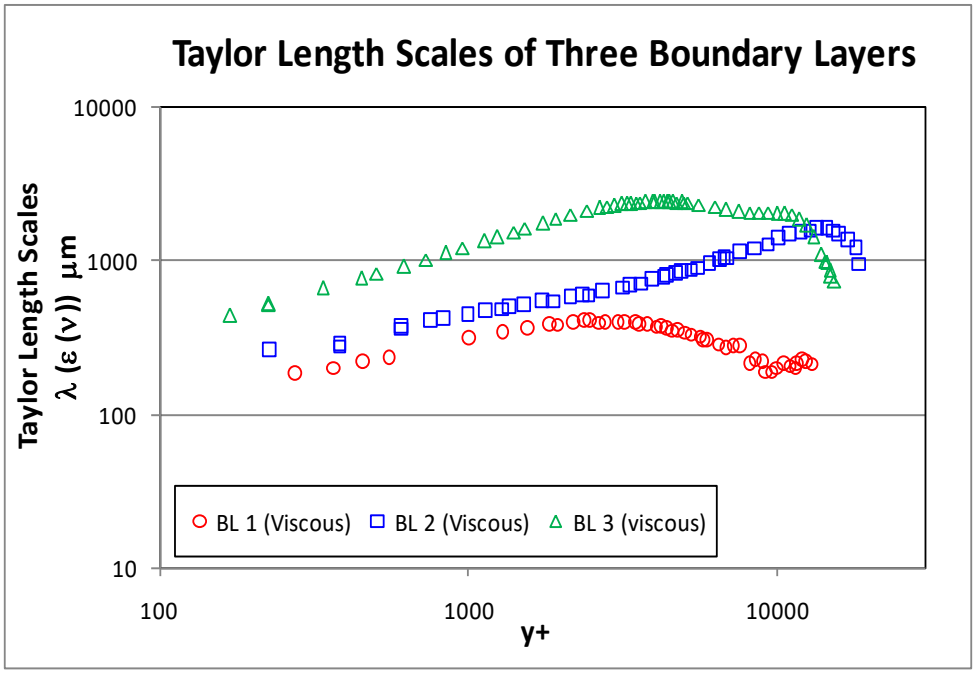

Figure 13. Logarithmic Taylor Length Scales through the Three Boundary Layers.

The integral length scales of the three boundary layers are particularly interesting since they exhibit changes in length scale that are can be explained due to the presence of the trip, vortex generators and uniform roughness. For example, Figure 14 shows the results of the integral length scales calculated from Eqn. 5 but using the energy dissipation ε(I) as determined from Eqn. 2 and plotted logarithmically against the non-dimensional wall units. The length scales for the clean tunnel boundary layer, BL1, are shown to be fairly constant, with a scale length of approximately 3.0 mm, up to y+ = 1900 and then reduces as the edge of the boundary layer approaches at y+ = 9500. This is typical of how the integral length scales behave in a 'clean' turbulent boundary layer.

However, with the inclusion of a trip and vortex generators, the integral length scales of boundary layer BL2 may be associated with the turbulence intensity values in Figure 7. Here the length scales closely follows those of the length scales of BL1 up to approximately y+ = 2700 and then deviates suggesting that the presence of these upstream obstacles have sustained the scale of the turbulence structures at approximately 3.0 mm throughout the boundary layer up to y+ = 13000 and only then falling off in value as the edge of the boundary layer approaches at y+

= 19000. It should be noted that the value of y+ = 2700 is the height of the 8 mm trip and the value of y+ = 13000 is the height of the vortex generators, similar to the findings of the turbulence intensity changes as given in Figure 7.

With the addition of the uniform roughness downstream of the trip and generators, the length scales of BL3 are initially of a higher magnitude to those BL1 and BL2 and remaining relatively constant at a value of approximately 5.0 mm up to a value of y+ = 2100, a value close to that of the height of the 8 mm trip. The increase in the length scale can be explained by considering the turbulence intensity results in Figure 7 whereon the turbulence is shown to be increasing with boundary layer height in the early stages unlike the results for BL1 and BL2, due to the uniform roughness elements. However, above y+ = 2100 the turbulence intensity, Figure 7, reduces monotonically as previously discussed and as the changes in the turbulence throughout the boundary layer, caused by the trip and generators, become more prominent, there is a reduction in the length scales. The rapid decline in the length scales beginning at y+ = 11000 towards the edge of the boundary layer at y+ = 15000 may be closely associated with the height of the generators.

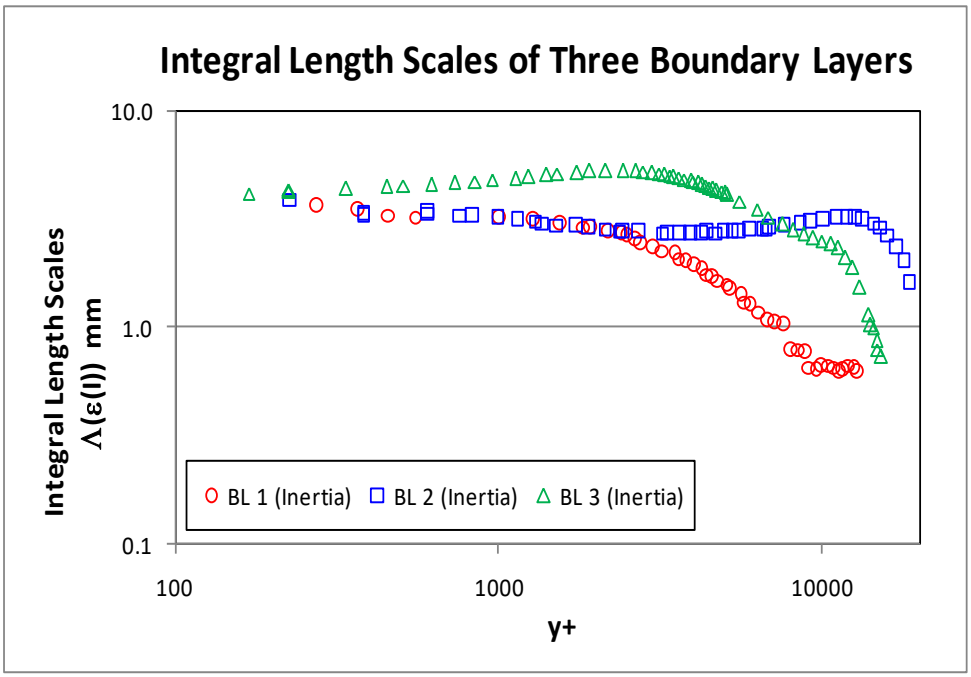

Figure 14. Logarithmic Integral Length Scales through the Three Boundary Layers.

By normalizing the data for the Law of the Wall and the three length scales for each of the boundary layers it is clearly shown that the inclusion of the trip, vortex generators and the roughness elements have a considerable effect on the original clean channel boundary layer. Although this result is not surprising in itself, it does shows how important it is for studies, experimental and numerical, to include upstream conditions within boundary layer development before embarking on determining data of complex flow regimes. For example, the normalized Law of the Wall for the three boundary layer conditions, Figure 15, provides evidence that the three boundary layers, BL1, BL2, and BL3, are in fairly good agreement with the universal Law of the Wall and as such would be acceptable for further studies to be considered. Even the

normalized Kolmogorov length scales for the three boundary layers are in good agreement with each other over the depth of the boundary layer in each case, Figure 16.

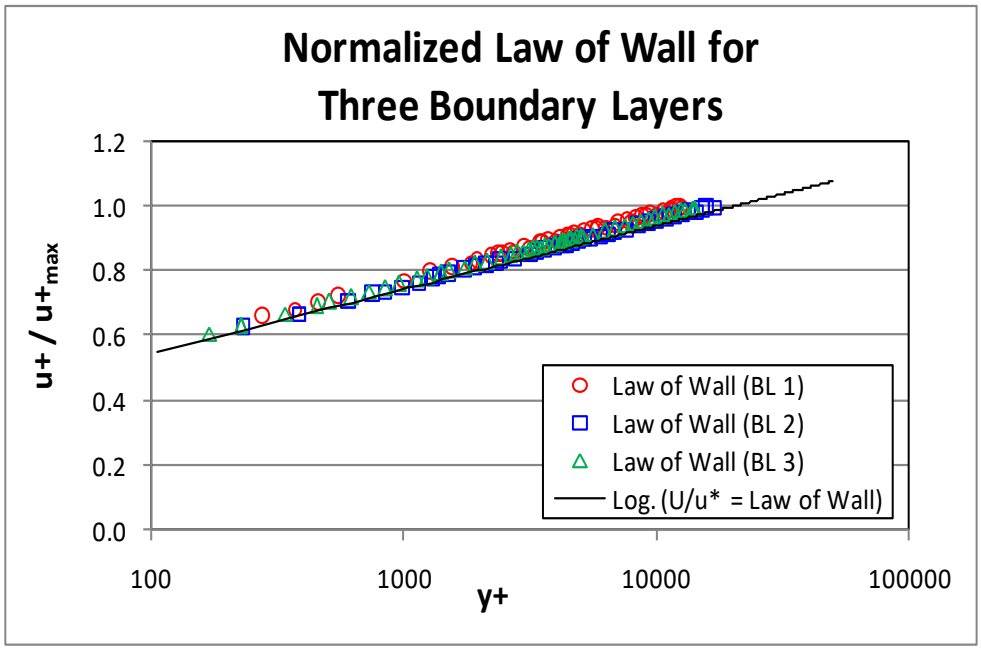

Figure 15. Comparison of the Law of the Wall of the Three Boundary Layers.

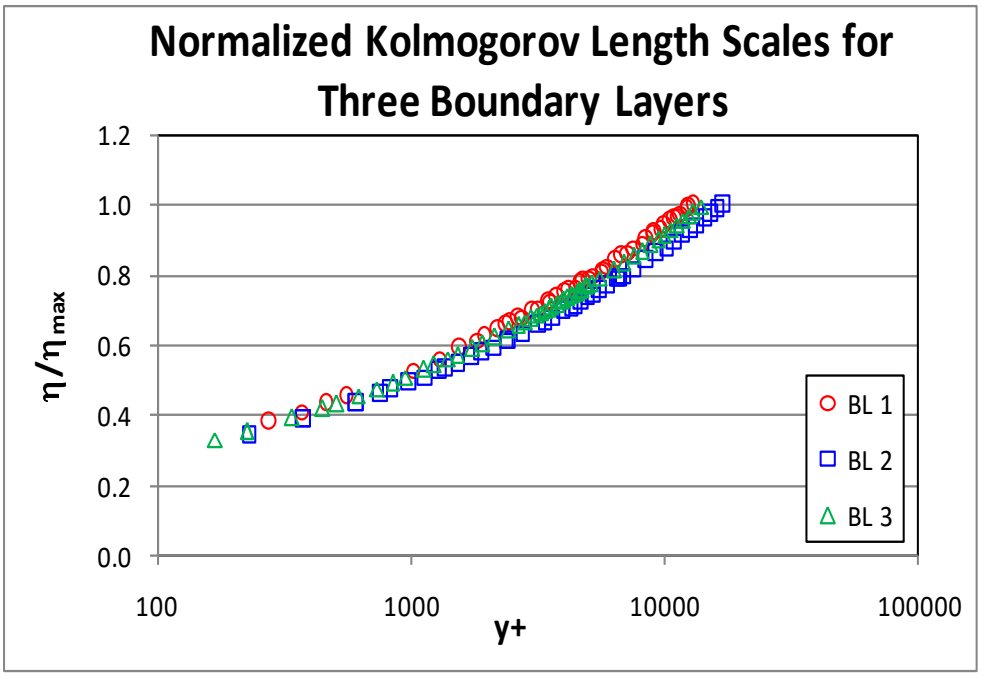

Figure 16. Comparison of the normalized Kolmogorov Length Scales of the Three Boundary Layers.

However, there is considerable difference for the normalized Taylor and Integral length scales throughout the three boundary layers as shown in Figures 17 and 18. Although the Taylor length

scales increase in value with the inclusion of, first the trip and vortex generators (BL2), and then the roughness elements (BL3), compared to the clean channel boundary layer (BL1) as shown in Figure 13, the normalized values provide a different picture. In this case it may be observed from Figure 17 that

(a) the position of peak change in the length scale for BL1 is y+ = 2400, that for BL2 is y+ = 13500 and for BL3 it is y+ = 4400, and

(b) the largest rate of change in length scale is that for BL1, whereas the lowest rate of change is for BL2 where the boundary layer is affected by the trip and the vortex generators, and

(c) the inclusion of the roughness elements appears to again increase this rate of change in the length scales of this boundary layer, BL3.

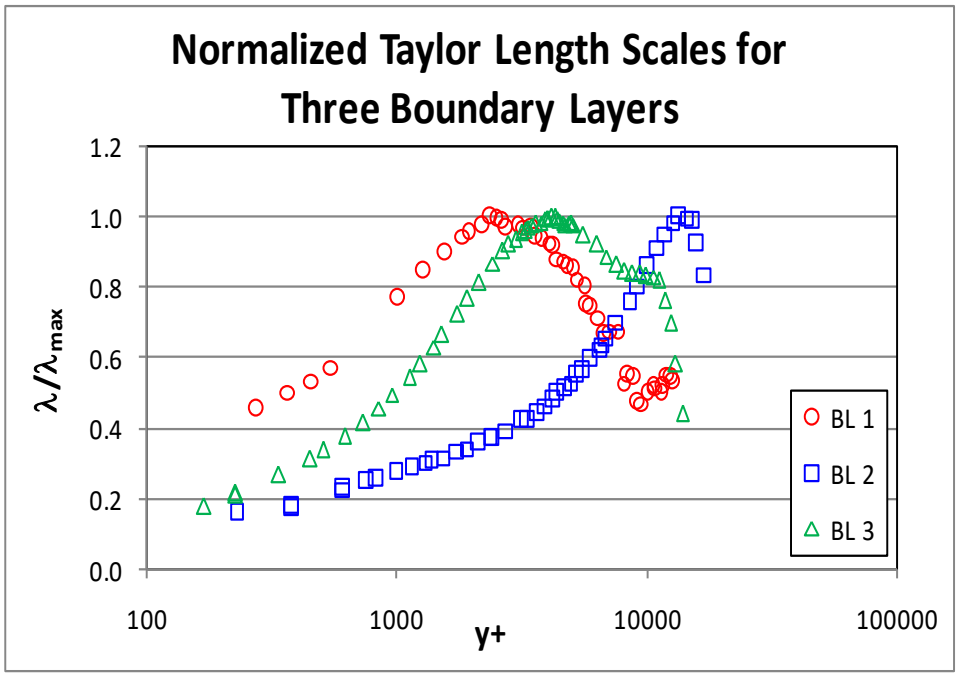

Figure 17. Comparison of the normalized Taylor Length Scales of the Three Boundary Layers.

The normalized Integral length scales for the three boundary layers, Figure 18, show that the length scales for BL1 is the largest at the start of the boundary layer and reduces in value throughout its depth which is as expected. However, the length scales for BL2 starts similar to that for BL1 with the largest length scales occurring at the start of the boundary layer and initially reducing in value in a comparable manner to that for BL1 up to y+ = 3600 and where they increase in value to a peak at y+ = 13000 (approximately the height of the vortex generators), where they then fall as the edge of the boundary layer approaches.

The length scales for BL3 start lower than that for the other two boundary layers even though it is affected by the inclusion of the roughness elements. However, the scales then increase and peak at approximately y+ = 2100, the height of the trip, and then reduce in value throughout the rest of the boundary layer with a very minor change in reduction in length scale at y+ = 11000 (the height of the vortex generators).

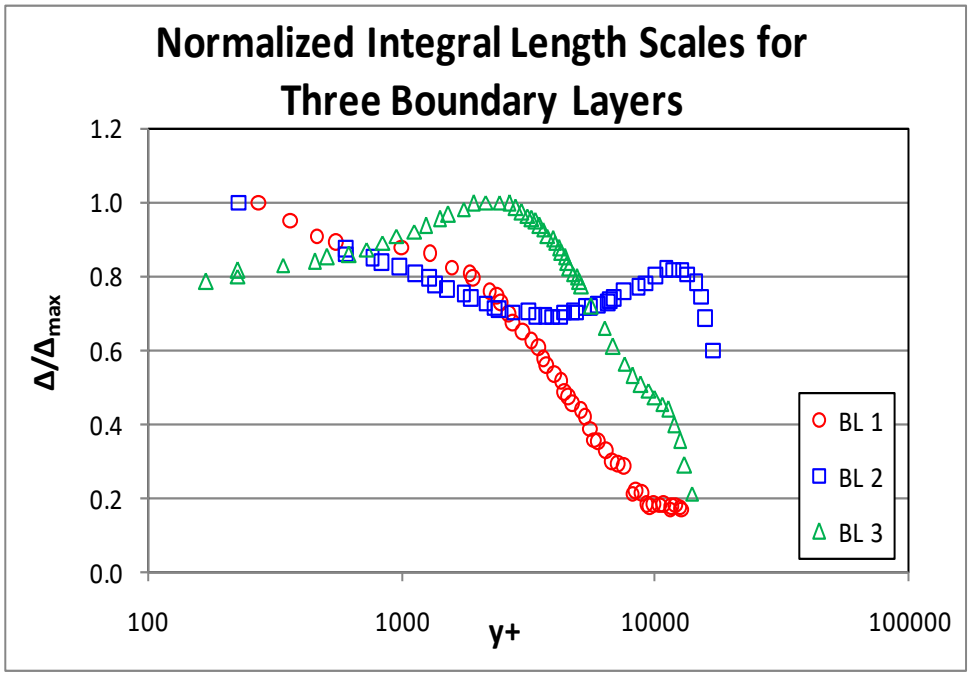

Figure 18. Comparison of the normalized Integral Length Scales of the Three Boundary Layers.

Table 3 provides a range of the length scales measured in the three boundary layers and shows that both the Kolmogorov and Taylor length scales increase in size throughout the boundary layer whereas the Integral length scale diminishes in value.

Table 3. Range of Length Scales for each of the Three Boundary Layers.

	Boundary Layer Configurations		
	BL1	BL2	BL3
Kolmogorov (η) μm	8 - 20	9 - 27	11 - 35
Taylor (λ) mm	0.18 - 0.40	0.25 - 1.60	0.40 - 2.40
Integral (Λ) mm	3.7 - 0.66	3.3 - 1.6	4.2 - 0.74

4. Conclusions

Three distinctly different turbulent boundary layers have been generated in a low subsonic test facility at Mach number, M = 0.49. The first boundary layer was allowed to develop naturally along the test section of a channel section, whereas two other boundary layers were developed from

a) the installation of a trip and vortex generators at the mouth of the facility, and

b) the inclusion of a uniform roughness fetch downstream of the vortex generators.

Temperature corrected hot-wire measurements were taken at a location far from the mouth of the facility where it was considered that the boundary layers would have had sufficient distance to develop into fully formed turbulent boundary layers. Velocity and turbulence profiles were obtained of the three boundary layers and their respective Kolmogorov, Taylor and Integral

length scales determined. It was found that the friction velocity was the largest in value for the clean tunnel boundary layer of 6.05 m/s and reduced in value to 5.04 m/s and 3.7 m/s as the turbulence increased within the next two boundary layers. This resulted in lowering the local skin friction coefficient for the three cases from 0.0026, to 0.0018 and 0.0010.

Although all three boundary layers were in agreement with the Law of the Wall, BL2 and BL3 exhibited a large departure from the Log Law line (Figure 9) because of the increased turbulence within the boundary layer due to the trip, vortex generators, and the uniform roughness elements.

This study has shown how important it is to take into account the flow regime from upstream obstacles when considering experimentally and/or numerically developing a strategy for enumerating flow conditions for a specific subject area, for example, studying the effect of a fire in an enclosed space and how to contain its spread or suppression.

References

[1] D. M. Shafer, Active and passive flow control over the flight deck of small naval vessels, MSc Thesis, Virginia Polytechnic Institute and State University, 2005.

[2] R. Bardera Mora, An Experimental Helicopter Wind Envelope for Ship Operations, International Journal of Mechanical, Aerospace, Industrial, Mechatronic and Manufacturing Engineering, vol 6(8), 2012.

[3] M. M. Wosnik, On wall-bounded turbulent shear flows, Thesis (PhD). State University of New York at Buffalow, Source DAI-B 61/09, pp. 4950, 2001.

[4] M. H. Buschmann and M. Gad-el-Hak, Recent developments in scaling of wall-bounded flows, Progress in Aerospace Sciences, vol 42(5-6), pp. 419-467, 2006.

[5] M. Schultz and K. Flack, The rough-wall turbulent boundary layer from the hydraulically smooth to the fully rough regime, Journal of Fluid Mechanics, vol 580, pp. 381-405, 2007.

[6] P. J. Disimile, J. M. Pyles, J. M. Davis and N. Toy, Aero-Optic Characterization of Multiple Free Shear Layers in a Backward Facing Step Flow, ESI, Inc Internal Report, 2008.

[7] Dantec Dynamics Technical Note, Improved Temperature Correction in StreamWare, Publication No: TN049909, 2002.

[8] N. Hutchins, T. B. Nickels, I Marusic and M. S. Chong, Hot-wire spatial resolution issues in wall-bounded turbulence, J. Fluid Mech., vol 635, pp. 103-136. 2009.

[9] H. Tennekes and J. L. Lumley, A First Course in Turbulence, The MIT Press, 1972.

[10] F. H. Clauser**,** Turbulent boundary layers in adverse pressure gradients, J. Aeronaut. Sci., vol 21, pp. 91-108, 1956.

[11] I. Marusic, R. Mathis and N. Hutchins, High Reynolds number effects in wall turbulence, International Journal of Heat and Fluid Flow, vol 31, pp. 418-428, 2010.

[12] J. P. Monty, J. A. Stewart, R. C Williams and M. S. Chong Large-scale features in turbulent pipe and channel flows J. Fluid Mech., vol 589, pp. 147-156, 2007.

Biographical information

Professor Peter J Disimile is an Associate Professor in Aerospace Engineering at the University of Cincinnati where he directs the Fire, Explosion, Science, and Technology research group. He earned his Ph.D. in Mechanical Engineering at Michigan State University with a primary focus on turbulent fluid dynamics and heat transfer. He has performed research in liquids and air under both single and multiphase conditions, at speeds ranging from 1 cm/sec to Mach 6. Peter is also a part-time SME for a small business, Engineering & Scientific Innovations, Inc., where he is responsible for the development of a "Smart High-speed Optical Fire Protection system" using artificial intelligence for the AF, and re-entrant jet and cavity dynamics produced by an underwater release for the Navy Strategic Programs Office.

Professor Norman Toy is a Consultant with Engineering & Scientific Innovations Inc. in Cincinnati but based in England, previously being a Visiting Professor in the Department of Aerospace Engineering at the University of Cincinnati, Ohio. Professor Toy received his B.Sc and Ph.D in Aeronautical Engineering from City University, London and then went to Surrey University in 1972 where he started as a Research Fellow in the Department of Mechanical Engineering, becoming a full Professor of Fluid Mechanics in the Department of Civil Engineering in 1994. His most recent research has focused on confined jets in a crossflow, hot surface ignition, hydrodynamic ram, flow visualization, as well as hydraulic jump in oscillating tanks.